coatings

MDPI

Communication

On the Asymmetry in Photo-Induced Motion of Graphene-Oxide Paper

Riccardo Castagna [1,2,*], Cristiano Riminesi [2,*], Andrea Di Donato [3], Rachele Castaldo [4], Roberto Avolio [4], Luigi Montalto [5], Francesco Vita [5], Oriano Francescangeli [5] and Daniele Eugenio Lucchetta [5,6,*]

1 URT-CNR@UNICAM, Laboratorio di Scienza e Tecnologia dei Materiali per la Fotonica e la Sensoristica Avanzata, PHOSMAT-Lab, Consiglio Nazionale delle Ricerche (CNR), Università degli Studi di di Camerino (UNICAM), Edifico "Carmelitane", Via Sant'Agostino, 1, 62032 Camerino, MC, Italy
2 CNR, Institute of Heritage Science, Via Madonna del Piano, 10, 50019 Sesto Fiorentino, FI, Italy
3 Dipartimento di Ingegneria dell'Informazione, Università Politecnica delle Marche, Via Brecce Bianche, 60131 Ancona, AN, Italy
4 IPCB-CNR, Via Campi Flegrei, 34, 80078 Pozzuoli, NA, Italy
5 Dipartimento di Scienze e Ingegneria della Materia dell'Ambiente ed Urbanistica (SIMAU), Università Politecnica delle Marche, Via Brecce Bianche, 60131 Ancona, AN, Italy
6 Optoacoustic Lab, Dipartimento di Scienze e Ingegneria della Materia dell'Ambiente ed Urbanistica (SIMAU), Università Politecnica delle Marche, Via Brecce Bianche, 60131 Ancona, AN, Italy
* Correspondence: riccardo.castagna@cnr.it (R.C.); cristiano.riminesi@cnr.it (C.R.); d.e.lucchetta@staff.univpm.it (D.E.L.)

Abstract: We report on the photo-mobility properties of a free standing large area graphene oxide (GO) paper (GOP). The thickness of the film is ≈20 µm. GOP is made by drop casting an aqueous suspension of GO on a microscope glass slide placed on a hot plate kept at the temperature of 70 °C. The film is peeled-off from the glass substrate and irradiated under different coherent and incoherent light sources. The film bends up to ≈55° when the irradiation is made using a near infra-red (NIR) incoherent incandescent lamp and returns back to the initial position when the NIR lamp is switched-off. The bending mechanism is attributed to the asymmetry of the GOP film obtained during the film formation process. We characterize the film morphology and structure using a Scanning Electron Microscopy (SEM) imaging and X-ray Diffraction (XRD) measurements, respectively. Remarkable differences between the two surfaces of the GOP are evidenced, both on a macroscopic length scale (surface roughness) and on a microscopic one (GO interlayer distance). This asymmetry results in different (negative) thermal expansion coefficients for the two film surfaces and hence in the bending of the film when the film temperature is increased by light absorption.

Keywords: photomobile film; graphene oxide; sensors; graphene oxide paper; contactless actuator

Citation: Castagna, R.; Riminesi, C.; Di Donato, A.; Castaldo, R.; Avolio, R.; Montalto, L.; Vita, F.; Francescangeli, O.; Lucchetta, D.E. On the Asymmetry in Photo-Induced Motion of Graphene-Oxide Paper. *Coatings* **2023**, *13*, 1310. https://doi.org/10.3390/coatings13081310

Academic Editor: Mihai Anastasescu

Received: 14 April 2023
Revised: 10 July 2023
Accepted: 21 July 2023
Published: 26 July 2023

1. Introduction

Composite polymer materials are widely used in many research fields [1–14]. They are also employed in the conversion of light into mechanical work that is achieved by photo-actuated films and devices based on azobenzene liquid crystals (LC) polymers [15–21]. Another way to convert light into work is represented by recently developed holographic photomobile polymer materials (H-PMP) where the motion can be realized by exploiting the light-induced Marangoni effect [22–28]. Concerning the azobenzene-based polymers, the light induced motion substantially depends on the cis-trans isomerization of the components [17]. More recently, the research focused on bilayered films made by coupling two layers with different photo-thermal expansion coefficients; this mismatch determines the bending of the film under irradiation and the restoration of the starting geometry when the light is switched-off [24–29]. In literature, a large variety of bilayered films made by carbon nano-tubes (CNTs) or by graphene-oxide (GO) is reported [29–40]. The effects of the temperature on different GO structures and geometries including ultrafast photo-induced

active ion transport through GO membranes are also widely studied [41–43]. It is worth to underline that a single thick GO paper (GOP) can behave as a double layered film if prepared in asymmetric configuration [44]. For instance, asymmetry may be induced during the film preparation by letting water evaporate at room temperature from an aqueous GO suspension drop-cast on a flat substrate. Here, we report on GOP prepared by using a relatively fast water evaporation at the temperature of 70 °C [44]. This temperature is below the reduction temperature of the GO (c.a. 150 °C) [45] X-ray diffraction (XRD) and Scanning Electron Microscopy (SEM) measurements performed on the two faces of the GO-film unequivocally demonstrate its asymmetric structure. A better understanding of the reasons of the bending mechanism will help the design of future sensors based on GO films. We show in this work that the asymmetry between the two surfaces of the GO film is responsible for the measured bending under light illumination. When irradiated with coherent and incoherent light the so prepared films exhibit a very fast bending that directly depends on the intensity of the light used [29].

2. Materials and Methods

2.1. Materials

GO water dispersion (4.5 mg/mL) is purchased from NANESA Co., Ltd. (Arezzo, Italy).

2.2. GO Film Preparation

A droplet (4 mL) of GO suspension is deposited on a glass slide placed on a hot plate at 70 °C for c.a. 15 min to obtain a c.a. 20 μm thick GOP. The layer is peeled-off by using a cutter and cut to obtain a 3 × 10 mm^2 rectangular stripe.

2.3. Optical Set-Up

An incoherent near infra-red (NIR) lamp is used to illuminate the film while a camera connected to an image acquisition system (IMAQ) detects each single frame up to a maximum resolution of 100 frames/s. The light intensity impinging on the sample is varied by changing the distance between the sample and the lamp. We used 5 and 10 cm as distance values. The corresponding measured light intensities impinging on the sample are 0.6, 0.2 W/cm^2. The effect of incoherent light is compared with that coming from a CW laser source at λ = 650 nm having power P = 120 mW and a beam radius r of about 2.5 mm (intensity 0.6 W/cm^2). Bending measurements are performed at 25 ± 1 °C.

2.4. SEM Imaging Measurements

A SEM Vega 3 TESCAN is used to detect and show the sample morphology. Samples are used without any conductive layer.

2.5. XRD-Measurements

The GOP is structurally characterized by XRD measurements performed by a Rigaku Smartlab 9 KW rotating anode diffractometer operating at λ = 1.54 angstrom in Bragg-Brentano configuration. Measurements are performed on both faces of GOP: on the upper face, with the film still attached to the glass substrate, and on the bottom face, with the film peeled-off. The conditions used for the X-ray analysys are: 2θ range 2–40 deg, step 0.04 deg, speed 4 deg/min.

2.6. Ultraviolet (UV)-Visible (VIS) Absorbance Measurements

UV-Vis spectra of the GO film are collected by using a Jasco V570 UV-Vis spectrophotometer in the 350–800 nm wavelengths range.

3. Results and Discussion

The preparation of the photomobile GOP (PM-GOP) follows a procedure in which a GO-suspension is deposited on a glass slide placed on a hot plate at 70 °C for ≈15 min. Figure 1 shows the GO-suspension at different times until the GO film is formed.

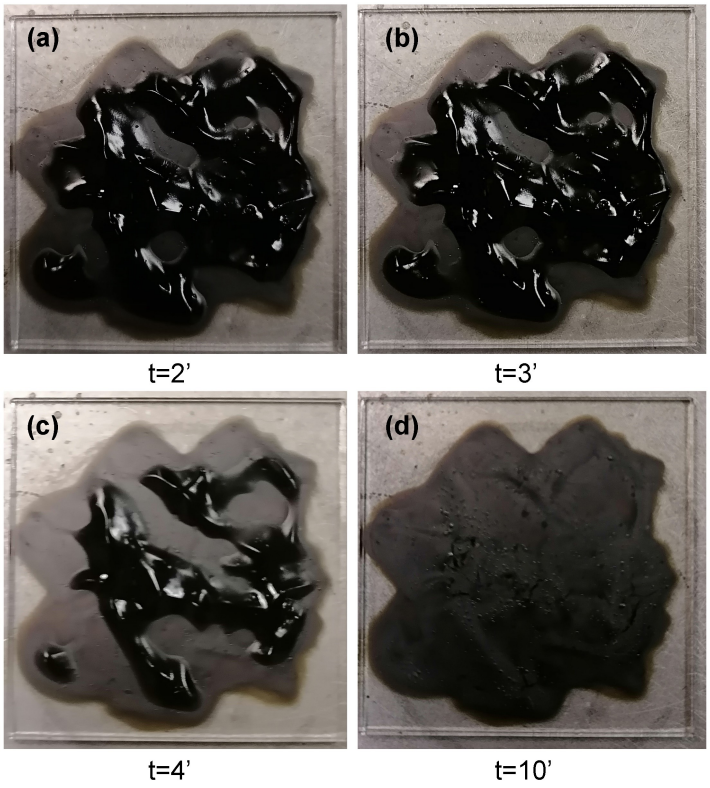

Figure 1. four images taken at different times during the water evaporation process until an homogeneous film of GO is obtained. (**a**), (**b**), (**c**) and (**d**) corresponds to 2, 3, 4 and 10 s respectively.

After that the PM-GOP is ready. The procedure is depicted in Figure 2 where the preparation steps and the final result are shown. Figure 3 represents the film bending under NIR incoherent radiation. The frames are taken at different times from a video showing the behaviour of the PM-GOP under NIR illumination when the distance between the lamp and the film is set to 5 cm. In order to clarify this behavior we performed a series of optical, morphological and structural measurements.

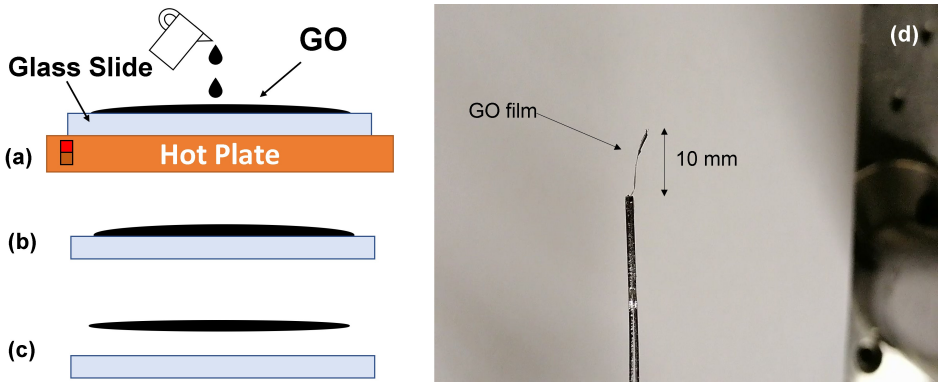

Figure 2. On the left side a sketch of the preparation process. In (**a**) GO is drop-cast on a glass substrate placed on a hot plate at 70 °C. In (**b**) the dried GO film is formed and in (**c**) the film is peeled-off from the substrate. On the right side (**d**) the final result ready to be illuminated.

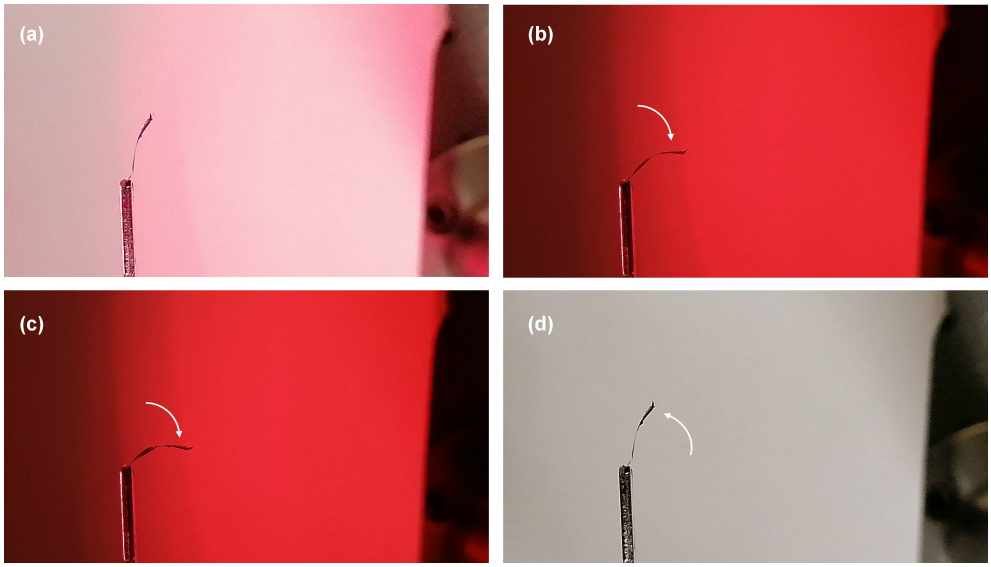

Figure 3. Frames taken at (**a**) 0, (**b**) 5 s, (**c**), 10 s, (**d**) 180 s during the irradiation with an incoherent NIR red light. Arrows indicate the direction of bending.

GO suspension (conc. 4.5 mg/mL; see Figure 4) shows a slightly decreasing absorption from VIS to NIR. Similar results are obtained when using the PM-GOP, as reported in literature [46]. The film is obtained in the conditions described in the experimental section and the UV-VIS spectra are collected. The photo-thermal conversion efficiency of the PM-GOPs in the NIR region is excellent [38,43]. This property explains the behavior of the PM-GOP film reported in Figure 5 where the angular displacement of the film is shown as a function of the time at two different distances from the used NIR light source. In the same figure, the relaxation process is shown when the impinging light is switched-off. As expected the PMP film tends to move back to its starting position showing that the entire process is reversible.

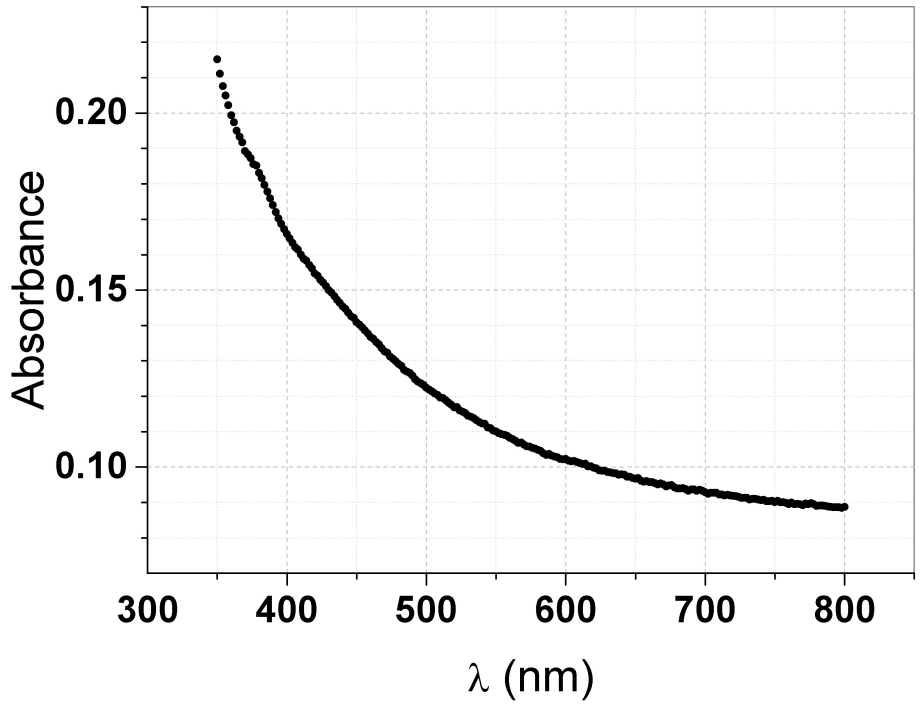

Figure 4. Absorbance of the GO suspension showing a slightly decreasing absorption in the VIS-NIR region.

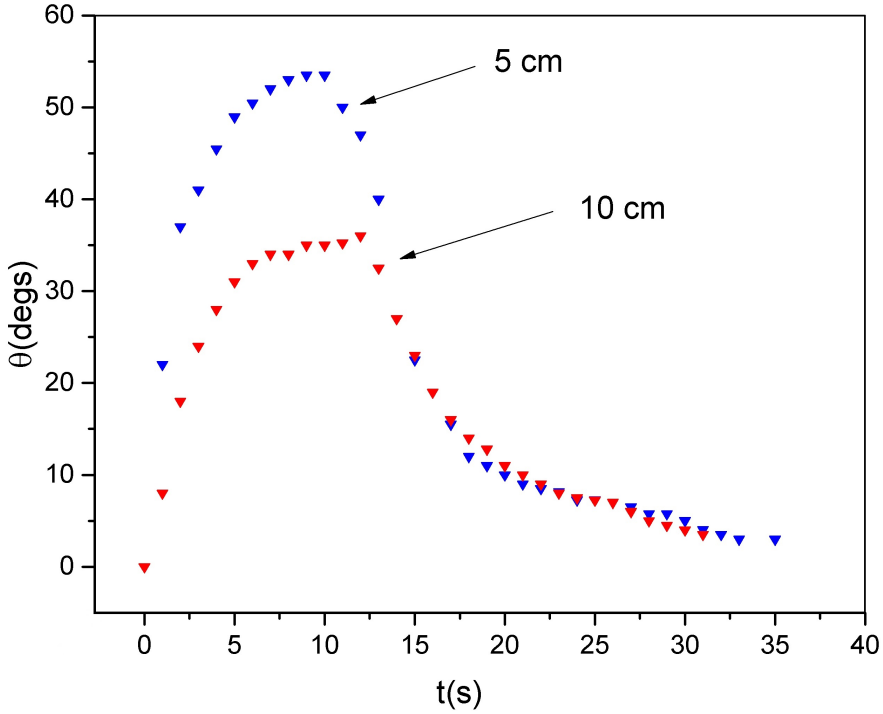

Figure 5. Angular displacement of the film as function of time when incoherent NIR illumination is used. Measurements are taken at two different distances, 5 (blue triangles) and 10 cm (red triangles) corresponding to 0.6 and 0.2 W/cm^2.

The measurement of the angular displacement as a function of time also shows that at shorter distances the film bends more and in a shorter time ≈55° in ≈10 s. With respect to the previous recently published manuscript (see ref. [29]) the motion of the GO film is, as expected, much faster and bending angles higher (see Table 1 in Supporting Information to compare bending angles and rates of different bilayered films). During the measurements and in controlled humidity conditions, the samples maintain their physical properties unaltered. Measurements are repeatable if the preparation procedure is carefully followed and if the experimental conditions are stable. By illuminating the sample with a coherent light the sample bends of ≈20 degrees in ≈2 s. The result is similar to that obtained with incoherent light placed at 10 cm from the sample, see Figure 6. However, the maximum achieved rotation angle is lower. This effect is due to the small irradiated area located near to the clamp. In other words a small fraction of the sample is illuminated and the bending results only from the change of the physical properties of the sample in that region The bending is due to the heating of the film by NIR [43]. We remark here that the film bends always with the concavity on the opaque face and the convexity on the shining one. In other words, the bending direction is the same independently from the direction of the impinging light. This property suggests that the film is asymmetric. The asymmetry of the film is here demonstrated by using SEM and XRD techniques. The SEM investigation reveals a remarkable morphological difference between the two sides of the GOP (see Figure 7) with a smooth morphology on the bottom surface, the one in touch with the smooth glass substrate during the film formation, and a reticulated one on the upper surface. It is evident that the morphology of the bottom surface is shaped by the smooth glass, while the upper one is dependent on the gel-air interface that is intrinsically irregular.

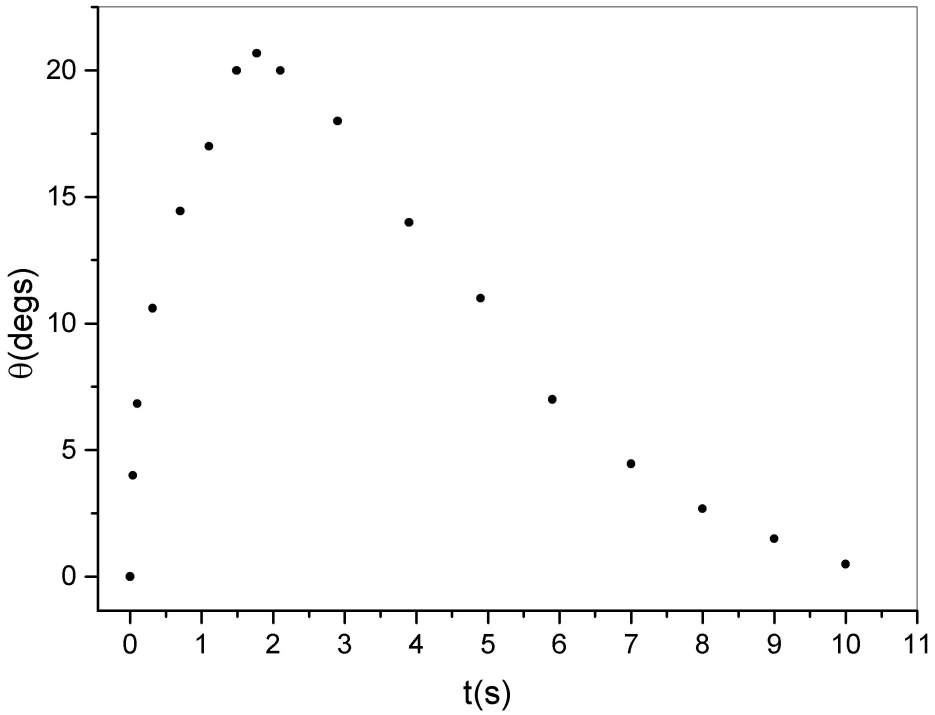

Figure 6. Angular displacement of the film as function of time when a low power coherent light is used to illuminate the film. Measurements are made by illuminating the base of the film.

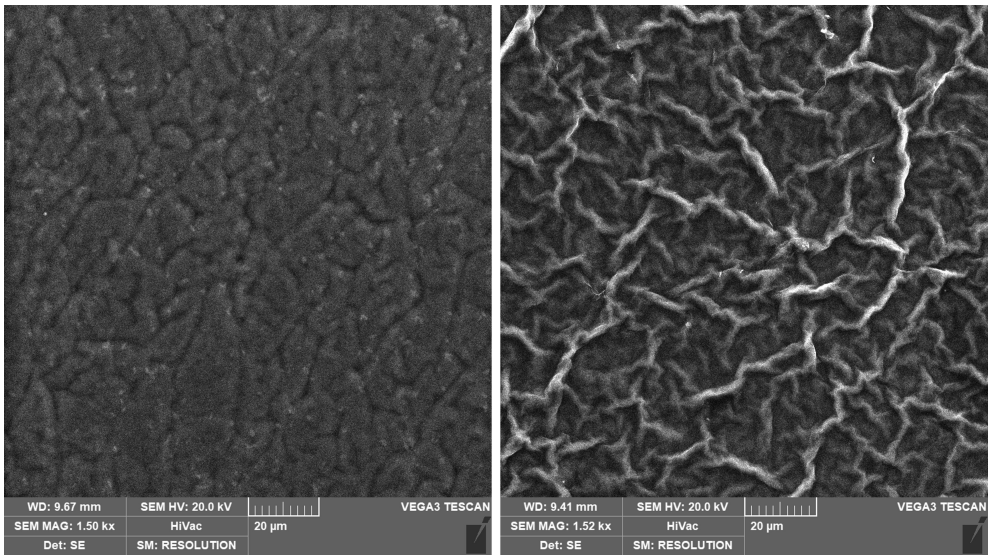

Figure 7. SEM images of the two sides of the film: the smooth shiny surface on the left, the rough opaque surface on the right.

XRD measurements show that the two faces of the film also differ on the molecular length scale (see Figure 8). The diffractogram taken on the opaque upper face is dominated by a peak at 2θ = 10.76 deg, characteristic of GO and corresponding to a d-spacing of 8.2 Å, the average distance among stacked GO planes [47]. However, the same measurement taken on the other face of the film shows a shift of the peak to a lower diffraction angle 2θ = 10.19 deg, corresponding to a slightly larger d-spacing of 8.7 Å. In both cases, no other peaks are observed, indicating the homogeneous oxidation of the layers (non-oxidized or reduced GO layers would exhibit a significantly smaller d-spacing of 4 Å [45]).

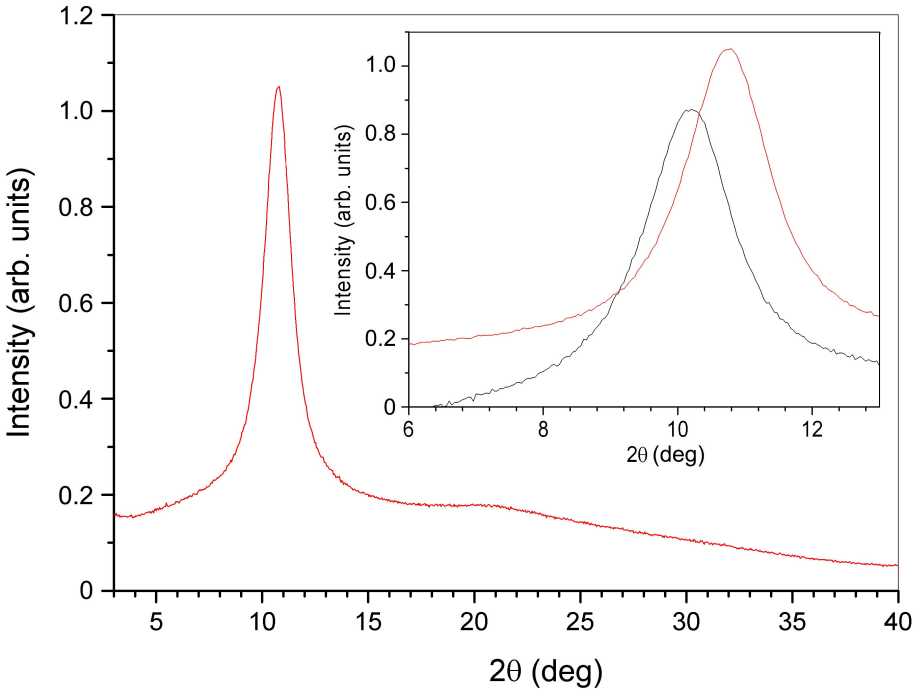

Figure 8. X-ray measurements made on both sides of the film. The red curve is referred to the upper (opaque) surface. The inset shows the comparison between the upper surface (in red) and the lower one (in black).

GOP are known to be highly hygroscopic, with the GO interlayer distance being extremely sensitive to the amount of water intercalated among hydrophilic GO layers [47]. In our case, the relatively large d-spacing values (larger than 8 Å on both faces) indicate the presence of some water throughout the whole film thickness [47,48], with a higher hydration in the face that is in contact with the glass substrate during the film preparation and hence farther from the evaporation surface. It is well known that the intercalated water plays a crucial role in determining the mechanical properties of GO films [49]. Also, the asymmetrical absorption of water by GO thin films may induce the creation of a gradient of humidity across the film, with the generation of expansion/compression stresses, which give rise to a bending moment to the GO film. Reduced graphene oxide (rGO) and rGO-clay hybrid thin films, for examples, were used to realize a humidity-sensitive electrical switching system in which the reversible actuation is due to water absorption and desorption due to joule effect [45]. The adsorption/desorption of water is responsible for its pseudonegative thermal expansion coefficient: according to the model described in Ref. [48], a reduction of temperature favors the adsorption of water between stacked GO layers, which in turn results in the swelling of the layers (increase of film thickness) and in their relative slipping (increase of the film area); the reverse effect occurs when heating causes water desorption.

On the base of this model, we ascribe the bending of our GO film to the different (negative) expansion coefficients of its two surfaces: light absorption determines an increase of temperature which favors water desorption and the consequent contraction of the film, with the top (opaque) face of the film exhibiting a larger (i.e., more negative) thermal expansion coefficient than the bottom (shiny) face; as a consequence, the opaque face of the films contracts more than the shiny face and the film bends with the concavity always on the opaque side.

Both the macroscopic and microscopic features of the film surfaces may contribute to their different thermal expansion coefficients. On the one hand, the higher roughness of the opaque face, hence its larger film-air interface, results in a facilitated desorption of water when the temperature increases and hence in a larger mechanical contraction compared to

the opposite face. On the other hand, the different interlayer distance on the two faces may affect the film response in a more complex way: while a larger d-spacing is expected to favor the water diffusion (because of the larger space available to the water molecules) and hence to lead to a larger thermal expansion coefficient for the shiny face than for the opaque face [48], other data reported in the literature indicate a thermal expansion coefficient that is more negative and lower the initial hydration of the film [50].

Indeed, the macroscopic expansion/contraction of GO film upon temperature changes depends in a nonlinear way from many experimental parameters, such as the initial water content in the film, the environment humidity, the rate of temperature change, the film thickness, etc. [48–50]. Further studies should be carried-out in order to better clarify the phenomenon and to elucidate the individual role of the macroscopic and microscopic properties of GO films in determining their photo-thermal response.

4. Conclusions

We studied the photo-thermally induced motion of a thin PM-GOP. The fact that the bending direction is independent of the direction of irradiation, clearly indicates that the origin of the effect resides in the film asymmetry induced by the drop-casting preparation process. In fact, a combination of SEM and XRD measurements shows that the two film faces differ at the macroscopic (opacity), micro-/nano-scopic (roughness) and sub-nanoscopic (GO-interlayer-spacing) levels. Such an asymmetry affects in a complex way the thermally induced adsorption/desorption of the water trapped in the GO film, eventually resulting in a different (negative) thermal expansion coefficients for the film to bend in response to a light-induced temperature increase.

Supplementary Materials: The following supporting information can be downloaded at: https://www.mdpi.com/article/10.3390/coatings13081310/s1.

Author Contributions: Conceptualization, R.C. (Riccardo Castagna) and D.E.L.; methodology, R.C. (Riccardo Castagna), D.E.L. and F.V.; software, A.D.D.; validation, R.C. (Riccardo Castagna), D.E.L. and F.V.; formal analysis, A.D.D. and F.V.; investigation, R.C. (Riccardo Castagna), D.E.L., R.C. (Rachele Castaldo), R.A., L.M. and F.V.; resources, R.C. (Riccardo Castagna) and C.R.; writing—original draft preparation, R.C. (Riccardo Castagna), D.E.L. and F.V.; writing—review and editing, D.E.L., R.C. (Riccardo Castagna), A.D.D. and F.V.; supervision, O.F., F.V., C.R., R.C. (Rachele Castaldo) and R.A.; project administration, C.R.; funding acquisition, R.C. (Riccardo Castagna) and C.R. All authors have read and agreed to the published version of the manuscript.

Funding: "Marche Applied Research Laboratory for Innovative Composites" (MARLIC), POR Marche FESR 2014–2020, Regione Marche (Italy). European Union—Next Generation EU. Project Code: ECS00000041; Project CUP: C43C22000380007; Project Title: Innovation, digitalization and sustainability for the diffused economy in Central Italy—VITALITY

Institutional Review Board Statement: Not applicable.

Informed Consent Statement: Not applicable.

Data Availability Statement: Data are available from the authors under reasonable request.

Acknowledgments: The authors thank the "Marche Applied Research Laboratory for Innovative Composites" (MARLIC), POR Marche FESR 2014–2020, Regione Marche (Italy) and European Union—Next Generation EU. Project Code: ECS00000041; Project CUP: C43C22000380007; Project Title: Innovation, digitalization and sustainability for the diffused economy in Central Italy—VITALITY.

Conflicts of Interest: The authors declare no conflicts of interest.

References

1. Biswal, T.; BadJena, S.K.; Pradhan, D. Synthesis of polymer composite materials and their biomedical applications. *Mater. Today Proc.* **2020**, *30*, 305–315. [CrossRef]
2. Tuttle, M. *Structural Analysis of Polymeric Composite Materials*, 2nd ed.; Taylor & Francis: Abingdon, UK, 2012.

3. Tsuchiya, H.; Asaki, Y.; Sinawang, G.; Asoh, T.A.; Osaki, M.; Park, J.; Ikemoto, Y.; Yamaguchi, H.; Harada, A.; Uyama, H.; et al. Cellulose Nanofiber Composite Polymeric Materials with Reversible and Movable Cross-links and Evaluation of their Mechanical Properties. *ACS Appl. Polym. Mater.* **2022**, *4*, 403–412.
4. Hsissou, R.; Seghiri, R.; Benzekri, Z.; Hilali, M.; Rafik, M.; Elharfi, A. Polymer composite materials: A comprehensive review. *Compos. Struct.* **2021**, *262*, 113640. [CrossRef]
5. Oladele, I.O.; Omotosho, T.F.; Adediran, A.A. Polymer-Based Composites: An Indispensable Material for Present and Future Applications. *Int. J. Polym. Sci.* **2020**, *2020*, 8834518. [CrossRef]
6. Vita, F.; Lucchetta, D.E.; Castagna, R.; Criante, L.; Simoni, F. Effects of resin addition on holographic polymer dispersed liquid crystals. *J. Opt. A Pure Appl. Opt.* **2009**, *11*, 024021. [CrossRef]
7. Lucchetta, D.; Vita, F.; Francescangeli, D.; Francescangeli, O.; Simoni, F. Optical measurement of flow rate in a microfluidic channel. *Microfluid. Nanofluidics* **2016**, *20*, 9. [CrossRef]
8. Lucchetta, D.; Spegni, P.; Di Donato, A.; Simoni, F.; Castagna, R. Hybrid surface-relief/volume one dimensional holographic gratings. *Opt. Mater.* **2015**, *42*, 366–369. Cited by: 6. [CrossRef]
9. Lucchetta, D.; Simoni, F.; Hernandez, R.; Mazzulla, A.; Cipparrone, G. Lasing from chiral doped nematic liquid crystal droplets generated in a microfluidic device. *Mol. Cryst. Liq. Cryst.* **2017**, *649*, 11–19. Cited by: 4. [CrossRef]
10. Lucchetta, D.E.; Castagna, R.; Simoni, F. Light-actuated contactless macro motors exploiting Bénard–Marangoni convection. *Opt. Express* **2019**, *27*, 13574–13580. [CrossRef]
11. Castagna, R.; Lucchetta, D.E.; Rippa, M.; Xu, J.H.; Donato, A.D. Near-frequency photons Y-splitter. *Appl. Mater. Today* **2020**, *19*, 100636.
12. Shalit, A.; Lucchetta, D.; Piazza, V.; Simoni, F.; Bizzarri, R.; Castagna, R. Polarization-dependent laser-light structured directionality with polymer composite materials. *Mater. Lett.* **2012**, *81*, 232–234.
13. Castagna, R.; Lucchetta, D.E.; Vita, F.; Criante, L.; Simoni, F. At a glance determination of laser light polarization state. *Appl. Phys. Lett.* **2008**, *92*, 041115. [CrossRef]
14. Rippa, M.; Castagna, R.; Pannico, M.; Musto, P.; Tkachenko, V.; Zhou, J.; Petti, L. Engineered plasmonic Thue-Morse nanostructures for LSPR detection of the pesticide Thiram. *Nanophotonics* **2017**, *6*, 1083–1092. .:10.1515/nanoph-2016-0146. [CrossRef]
15. Yu, Y.; Nakano, M.; Ikeda, T. Directed bending of a polymer film by light. *Nature* **2003**, *425*, 145. [CrossRef]
16. Zhou, Y.; Wang, L.; Ma, S.; Zhang, H. Fully Room-Temperature Reprogrammable, Reprocessable, and Photomobile Soft Actuators from a High-Molecular-Weight Main-Chain Azobenzene Crystalline Poly(ester-amide). *ACS Appl. Mater. Interfaces* **2022**, *14*, 3264–3273.
17. Chiellini, E.; Galli, G.; Altomare, A.; Solaro, R.; Angeloni, A.; Laus, M.; Carlini, C.; Caretti, D. Thermotropic and solution photoisomerization properties of side-chain liquid crystalline polymers containing methyl-substituted azobenzene mesogens. *Mol. Cryst. Liq. Cryst. Sci. Technol. Sect. A Mol. Cryst. Liq. Cryst.* **1992**, *221*, 61–69. [CrossRef]
18. Yamada, M.; Kondo, M.; Mamiya, J.i.; Yu, Y.; Kinoshita, M.; Barrett, C.J.; Ikeda, T. Photomobile polymer materials: Towards light-driven plastic motors. *Angew. Chem.* **2008**, *120*, 5064–5066. [CrossRef]
19. Ube, T.; Ikeda, T. Photomobile Polymer Materials with Complex 3D Deformation, Continuous Motions, Self-Regulation, and Enhanced Processability. *Adv. Opt. Mater.* **2019**, *7*, 1900380. [CrossRef]
20. Ikeda, T.; Ube, T. Photomobile polymer materials: From nano to macro. *Mater. Today* **2011**, *14*, 480–487. [CrossRef]
21. Koerner, H.; White, T.J.; Tabiryan, N.V.; Bunning, T.J.; Vaia, R.A. Photogenerating work from polymers. *Mater. Today* **2008**, *11*, 34–42. [CrossRef]
22. Castagna, R.; Nucara, L.; Simoni, F.; Greci, L.; Rippa, M.; Petti, L.; Lucchetta, D.E. An Unconventional Approach to Photomobile Composite Polymer Films. *Adv. Mater.* **2017**, *29*, 1604800. [CrossRef] [PubMed]
23. Lucchetta, D.E.; Simoni, F.; Sheremet, N.; Reshetnyak, V.; Castagna, R. Shape-driven optofluidic rotational actuation. *Eur. Phys. J. Plus* **2021**, *136*, 445. [CrossRef]
24. Lucchetta, D.; Di Donato, A.; Singh, G.; Tombesi, A.; Castagna, R. Optically tunable diffraction efficiency by photo-mobile holographic composite polymer material. *Opt. Mater.* **2021**, *121*, 111612. [CrossRef]
25. Lucchetta, D.E.; Castagna, R.; Singh, G.; Riminesi, C.; Di Donato, A. Spectral, morphological and dynamical analysis of a holographic grating recorded in a photo-mobile composite polymer mixture. *Nanomaterials* **2021**, *11*, 2925.
26. Lucchetta, D.E.; Di Donato, A.; Paturzo, M.; Singh, G.; Castagna, R. Light-Induced Dynamic Holography. *Micromachines* **2022**, *13*, 297. [CrossRef]
27. Castagna, R.; Donato, A.D.; Strangi, G.; Lucchetta, D.E. Light controlled bending of a holographic transmission phase grating. *Smart Mater. Struct.* **2022**, *31*, 03LT02. [CrossRef]
28. Lucchetta, D.E.; Di Donato, A.; Francescangeli, O.; Singh, G.; Castagna, R. Light-Controlled Direction of Distributed Feedback Laser Emission by Photo-Mobile Polymer Films. *Nanomaterials* **2022**, *12*, 2890. [CrossRef]
29. Castagna, R.; Di Donato, A.; Castaldo, R.; Avolio, R.; Francescangeli, O.; Lucchetta, D.E. Scotch-Tape and Graphene-Oxide Photomobile Polymer Film. *Photonics* **2022**, *9*, 659. [CrossRef]
30. Pillai, V.V.S.; Kumari, P.; Benedetto, A.; Gobbo, D.; Ballone, P. Absorption of Phosphonium Cations and Dications into a Hydrated POPC Phospholipid Bilayer: A Computational Study. *J. Phys. Chem. B* **2022**, *126*, 4272–4288.
31. Papadimopoulos, A.N.; Kantartzis, N.V.; Tsitsas, N.L.; Valagiannopoulos, C.A. Wide-angle absorption of visible light from simple bilayers. *Appl. Opt.* **2017**, *56*, 9779–9786. [CrossRef]

32. Hu, Y.; Qi, K.; Chang, L.; Liu, J.; Yang, L.; Huang, M.; Wu, G.; Lu, P.; Chen, W.; Wu, Y. A bioinspired multi-functional wearable sensor with an integrated light-induced actuator based on an asymmetric graphene composite film. *J. Mater. Chem. C* **2019**, *7*, 6879–6888. [CrossRef]
33. Kim, S.; Jung, H.J.; Kim, J.C.; Lee, K.S.; Park, S.S.; Dravid, V.P.; He, K.; Jeong, H.Y. In Situ Observation of Resistive Switching in an Asymmetric Graphene Oxide Bilayer Structure. *ACS Nano* **2018**, *12*, 7335–7342.
34. Zhang, Y.; Jiang, H.; Li, F.; Xia, Y.; Lei, Y.; Jin, X.; Zhang, G.; Li, H. Graphene oxide based moisture-responsive biomimetic film actuators with nacre-like layered structures. *J. Mater. Chem. A* **2017**, *5*, 14604–14610. [CrossRef]
35. Kim, J.; Cote, L.J.; Huang, J. Two Dimensional Soft Material: New Faces of Graphene Oxide. *Accounts Chem. Res.* **2012**, *45*, 1356–1364.
36. Kumar, N.; Srivastava, V.C. Simple Synthesis of Large Graphene Oxide Sheets via Electrochemical Method Coupled with Oxidation Process. *ACS Omega* **2018**, *3*, 10233–10242.
37. Lai, Q.; Zhu, S.; Luo, X.; Zou, M.; Huang, S. Ultraviolet-visible spectroscopy of graphene oxides. *AIP Adv.* **2012**, *2*, 032146,
38. Wu, C.; Feng, J.; Peng, L.; Ni, Y.; Liang, H.; He, L.; Xie, Y. Large-area graphene realizing ultrasensitive photothermal actuator with high transparency: New prototype robotic motions under infrared-light stimuli. *J. Mater. Chem.* **2011**, *21*, 18584–18591. [CrossRef]
39. Zhang, E.; Wang, T.; Hong, W.; Sun, W.; Liu, X.; Tong, Z. Infrared-driving actuation based on bilayer graphene oxide-poly(N-isopropylacrylamide) nanocomposite hydrogels. *J. Mater. Chem. A* **2014**, *2*, 15633–15639. [CrossRef]
40. Hu, Y.; Wu, G.; Lan, T.; Zhao, J.; Liu, Y.; Chen, W. A Graphene-Based Bimorph Structure for Design of High Performance Photoactuators. *Adv. Mater.* **2015**, *27*, 7867–7873.
41. Yang, J.; Hu, X.; Kong, X.; Jia, P.; Danyan, J.; Quan, D.; Wang, L.; Wen, Q.; Lu, D.; Jiang, L.; et al. Photo-induced ultrafast active ion transport through graphene oxide membranes. *Nat. Commun.* **2019**, *10*, 1171. [CrossRef]
42. Qu, Y.; Yang, Y.; Wu, J.; Zhang, Y.; Jia, L.; El Dirani, H.; Crochemore, R.; Sciancalepore, C.; Demongodin, P.; Grillet, C.; et al. Photo-Thermal Tuning of Graphene Oxide Coated Integrated Optical Waveguides. *Micromachines* **2022**, *13*, 1194. [CrossRef]
43. Bae, J.J.; Yoon, J.H.; Jeong, S.; Moon, B.H.; Han, J.T.; Jeong, H.J.; Lee, G.W.; Hwang, H.R.; Lee, Y.H.; Jeong, S.Y.; et al. Sensitive photo-thermal response of graphene oxide for mid-infrared detection. *Nanoscale* **2015**, *7*, 15695–15700. [CrossRef]
44. Cheng, H.; Zhao, F.; Xue, J.; Shi, G.; Jiang, L.; Qu, L. One Single Graphene Oxide Film for Responsive Actuation. *ACS Nano* **2016**, *10*, 9529–9535.
45. Castaldo, R.; Lama, G.C.; Aprea, P.; Gentile, G.; Ambrogi, V.; Lavorgna, M.; Cerruti, P. Humidity-Driven Mechanical and Electrical Response of Graphene/Cloisite Hybrid Films. *Adv. Funct. Mater.* **2019**, *29*, 1807744,
46. Khan, M.; Al-Marri, A.H.; Khan, M.; Mohri, N.; Adil, S.F.; Al-Warthan, A.; Siddiqui, M.R.H.; Alkhathlan, H.Z.; Berger, R.; Tremel, W.; et al. Pulicaria glutinosa plant extract: A green and eco-friendly reducing agent for the preparation of highly reduced graphene oxide. *RSC Adv.* **2014**, *4*, 24119–24125. [CrossRef]
47. Iakunkov, A.; Talyzin, A.V. Swelling properties of graphite oxides and graphene oxide multilayered materials. *Nanoscale* **2020**, *12*, 21060–21093. [CrossRef]
48. Zhu, J.; Andres, C.M.; Xu, J.; Ramamoorthy, A.; Tsotsis, T.; Kotov, N.A. Pseudonegative Thermal Expansion and the State of Water in Graphene Oxide Layered Assemblies. *ACS Nano* **2012**, *6*, 8357–8365.
49. Compton, O.C.; Cranford, S.W.; Putz, K.W.; An, Z.; Brinson, L.C.; Buehler, M.J.; Nguyen, S.T. Tuning the Mechanical Properties of Graphene Oxide Paper and Its Associated Polymer Nanocomposites by Controlling Cooperative Intersheet Hydrogen Bonding. *ACS Nano* **2012**, *6*, 2008–2019.
50. Su, Y.; Wei, H.; Gao, R.; Yang, Z.; Zhang, J.; Zhong, Z.; Zhang, Y. Exceptional negative thermal expansion and viscoelastic properties of graphene oxide paper. *Carbon* **2012**, *50*, 2804–2809. [CrossRef]